PCCP

Subpicosecond HI Elimination in the 266 nm Photodissociation of Branched Iodoalkanes

Journal:	*Physical Chemistry Chemical Physics*
Manuscript ID	CP-ART-11-2019-006460.R2
Article Type:	Paper
Date Submitted by the Author:	29-Sep-2020
Complete List of Authors:	Todt, Michael; Cornell University, Department of Chemistry and Chemical Biology Datta, Sagnik; Cornell University, Department of Chemistry and Chemical Biology Rose, Alex; Cornell University, Department of Chemistry and Chemical Biology Leung, Kiana; Cornell University, Department of Chemistry and Chemical Biology Davis, H.; Cornell University

Subpicosecond HI Elimination in the 266 nm Photodissociation of Branched Iodoalkanes

Received xx
Accepted xx

DOI: 10.1039/x0xx00000x

Michael A. Todt[a], Sagnik Datta[a], Alex Rose[a], Kiana Leung[a], and H. Floyd Davis[a,b]

The 266 nm photodissociation dynamics of 1-iodopropane and 2-iodopropane were studied using photofragment translational energy spectroscopy using vacuum ultraviolet (VUV) photoionization and electron impact ionization detection of products. The photochemistry of 1-iodopropane was found to be similar to that of iodomethane and iodoethane, with dominant production of $I^*(^2P_{1/2})$, and no evidence (< 0.21%) for HI + alkene formation. Significantly different behavior was observed for 2-iodopropane, with dominant production of ground state $I(^2P_{3/2})$, and a HI yield > 10.5%. The anisotropy (β) parameters for all channels approached the limiting value of 2.0, indicating that 1,2-HI elimination occurs on subpicosecond timescales, like direct C-I bond fission, following excitation to $^3Q_0$. The HI translational energy and angular distributions were similar to those for $I(^2P_{3/2})$, suggesting that motion of the heavy I atom in HI is largely derived from the repulsive nature of the $^1Q_1$ surface correlating to R + I with the light H atom picked up by ground state I late in the exit channel producing highly vibrationally excited HI.

Introduction

The ultraviolet photodissociation of iodoalkanes in the first absorption band (A band) has been an active area of study for many decades, with CH_3I having been investigated most extensively.[1] Early studies by Riley and Wilson employed photofragment translational energy spectroscopy with electron impact ionization mass spectrometric detection of products.[2] With several exceptions,[3,4,5,6] most subsequent studies have employed ion and velocity map imaging detection of the iodine atom and hydrocarbon radical fragments.[7-15]

Iodoalkanes containing one to four carbon atoms have similar unstructured UV absorption spectra (λ_{max} ~ 260 nm).[12,16] Photoexcitation populates mainly the repulsive $^3Q_0$ state, dissociating directly to produce spin-orbit-excited state $I^*(^2P_{1/2})$. As illustrated in Fig. 1, nonadiabatic crossing to the repulsive $^1Q_1$ surface leads to ground state $I(^2P_{3/2})$. Direct absorption to the $^3Q_1$ surface also occurs via a weak perpendicular transition primarily to the red of 260 nm for both branched and linear iodoalkanes.[7,9] A direct perpendicular transition to the $^1Q_1$ state also occurs to the blue of 260 nm for linear Iodoalkanes.

Pathways other than C-I bond fission have received remarkably little attention. Continetti, Balko and Lee reported a minor (~ 3%) C-H bond fission channel in CH_3I photodissociation at 193 nm.6 Ross and Johnston observed HI peaks in TOF mass spectra recorded following 248 nm photolysis of iodoalkanes; however, product branching ratios, angular distributions, and kinetic energy distributions were not determined.[17]

Here, we report that HI elimination plays a significant role in the photodissociation of branched iodoalkanes at 266 nm. A particularly intriguing finding is that the HI angular and translational energy distributions are quite similar to those for $I(^2P_{3/2})$, indicating that the HI elimination channel is direct, occurring on subpicosecond timescales. This contrasts with most previous examples of HX elimination, which typically proceed on ground electronic state surfaces, following internal conversion.[18-23]

Experimental Methods

The experiments were carried out using a rotatable source crossed molecular beams apparatus equipped with both vacuum ultraviolet (VUV) photoionization and electron impact ionization detection.[24] This apparatus, originally using synchrotron radiation for photoionization, has been reconfigured at Cornell University using pulsed 8.8-11.9 eV light generated using tabletop nanosecond pulsed lasers.[25,26]

The molecular beams (~ 2% in He at ~ 1000 Torr) were generated by room temperature dual-piezoelectrically actuated pulsed valves operating at 30 Hz.[27] For the determination of the I:I* branching ratios, the 1-iodopropane beam was run in the primary source and 2-iodopropane run in the secondary source, making it possible to compare photodissociation signals for each isomer under identical photoionization conditions. The pulsed valve timing was adjusted so that photolysis occurred in the warmer, early part of the molecular beam pulse to minimize interference by photodissociation of van der Waals clusters. A fraction of the photodissociation products drifted a fixed distance (15.0 cm or 32.8 cm for photoionization and electron impact ionization, respectively) from the main chamber ($P < 10^{-6}$ Torr during experiment) through three regions of differential pumping to the liquid-nitrogen cooled ionization region of the

[a] Department of Chemistry and Chemical Biology, Baker Laboratory, Cornell University, Ithaca, NY 14853-1301

[b] Author to whom correspondence should be addressed at hfd1@cornell.edu

[c] Electronic supplementary information (ESI) available: PDF file containing (i) Determination of the Anisotropy Parameters (β) for the different photodissociation channels, and their respective error limits, ii) Relationship between excited state lifetime (τ), anisotropy parameter (β), and rotational temperature (T), iii) Polarization TOFs and determination of β for the $I(^2P_{3/2}) + C_3H_7$ channel from 1-C_3H_7I photodissociation, and iv) Polarization TOFs and determination of β for the $I^* + C_3H_7$ channel from 2-C_3H_7I photodissociation

[d] . See DOI: 10.1039/x0xx00000x.

UHV detector, typically maintained at pressures below 1 x 10^{-10} Torr during the experiment.[24] An Extrel quadrupole mass spectrometer with Daly ion detector was utilized for the detection of the photodissociation products.

Using 70 eV electron impact ionization detection, time-of-flight (TOF) spectra were recorded for C_3H_7, C_3H_6, HI, I and I* products from 1- and 2-C_3H_7I photodissociation. For photoionization detection of I*, HI, C_3H_7, and C_3H_6, single photon ionization near 125 nm (9.9 eV) was used in most experiments. Vacuum ultraviolet light was produced via four-wave sum-frequency mixing of collimated (unfocused) dye lasers, employing the two-photon resonance (312.85 nm) in Hg.[25,26] Ground state I products were ionized by 1+1' resonance enhanced multiphoton ionization (REMPI) through the $5s^25p^4(^3P_2)8s\ ^2[2]_{3/2}$ state at 128.94 nm (9.6 eV). As described in detail below, for determination of the I:I* branching ratios, I* alone was ionized by single photon ionization near 128.94 nm with the laser tuned 5 cm^{-1} off of the I atom REMPI resonance. We also carried out studies of the HI products using 9.6 and 8.8 eV photoionization.

Analyses of the product TOF distributions were carried out using SBEAM, an iterative forward convolution program written at Cornell. The program takes the known parameters of the crossed beams apparatus and molecular beam, as well as user-generated product translational energy distributions, P(E), and the anisotropy parameter, β, as inputs.[28] The translational energy P(E) and angular I(θ) functions were assumed to be separable, i.e., P(E, θ) = P(E) x I(θ) for each channel. This assumption was subsequently verified by our ability to adequately simulate the TOF and polarization angular distributions. For a single photon absorption process, the photofragment angular distribution, I(θ), can be expressed as

$$I(\theta) = \frac{1}{4\pi}\left(1 + \beta P_2(\cos\theta)\right) \qquad (1)$$

where β = 2.0 for a pure parallel transition, β = -1.0 for a pure perpendicular transition, $P_2(\cos\theta)$ is the second order Legendre polynomial in cos θ, and θ is the angle between fragment recoil direction and polarization direction.[29] Using a trial P(E) and β as inputs, the program calculated TOF spectra and angular distributions for comparison to the experimental data. An "on the fly" graphical user interface allows the input parameters to be adjusted while the calculated TOF spectra are updated in real time and superimposed on the experimental data.

In order to ensure that the signal attributed to HI elimination at m/e = 128 does not result from imperfect mass resolution, *i.e.*, from spillover from I^+ signal at m/e = 127, we studied the photodissociation of CF_3I at 266 nm, using 70 eV electron impact ionization and photoionization. Since CF_3I dissociates to CF_3 + I and cannot produce HI, signal observed at m/e = 128 in the CF_3I experiment must result from spillover from m/e = 127. Under our experimental conditions, spillover at m/e = 128 was found to be 1.56% using CF_3I and utilizing 70 eV electron impact ionization. Similarly, for the photoionization experiments, the spillover at m/e = 128 was found to be 3.6%. In order to fully correct for spillover, the measured I atom TOF spectra were multiplied by the above percentages and then subtracted from corresponding HI TOF spectra prior to forward convolution analysis of the HI data.

An unseeded (~1 cm^{-1} bandwidth) Continuum Powerlite 9030 Nd:YAG laser was used for photolysis at 266 nm. A half-waveplate mounted in a precision rotation stage was placed in the path of the 266 nm laser beam in order to rotate the polarization of the photolysis beam relative to the detector axis. The polarization was analyzed and verified using a Glan-Taylor polarizing prism. In order to determine the anisotropy parameter (β), for each detected species, TOF spectra were recorded at a specific lab angle (10^o) at polarization angles corresponding to the observed maximum and minimum signal levels. Additional TOF spectra were recorded at intermediate polarization angles. Most experiments were conducted using 10 mJ pulses focused to ~ 3 mm diameter, but lower energies were used in the polarization studies. Power dependence studies showed a linear dependence of signal on laser power and no dependence of the shapes of TOF spectra on laser power, thereby demonstrating single photon absorption.

The anisotropy parameters (β) were derived through the iterative forward convolution process utilizing the previously determined product translational energy distributions, P(E), to simulate measured TOF spectra recorded for various channels at different polarization angles. The integrated experimental signal intensities for the forward peak of the TOF spectra at various polarization angles were also compared to calculated intensities.

Since TOF spectra represent cuts through Newton circles sampling specific center of mass recoil angles, our ability to simulate the relative contributions to the "forward" and "backward" portions of the TOF spectra provides a good cross check to the accuracy of our derived values of β. It also provides the means to identify possible dependence of β on the translational energy distribution, P(E).

Time-of-flight data shown in this paper for C_3H_7, I* and HI were recorded using single photon VUV photoionization at 9.9 eV and 9.6 eV. Data for I were recorded using REMPI VUV photoionization at 9.6 eV. The experimental TOFs at different lab angles for C_3H_6 and HI were also recorded using electron impact ionization at 70 eV. Polarization studies for HI were recorded using single photon VUV photoionization at 9.9 eV; additional HI TOF studies were carried out at 9.6 and 8.8 eV.

Results and Discussion

The TOF spectra for C_3H_7, I and I* from 1-C_3H_7I photodissociation with the photolysis laser polarization parallel to the detector axis using photoionization detection, are shown in Fig. 2. The solid lines represent calculated TOF spectra, using the P(E) distributions from Fig. 3, and optimized anisotropy parameters β = 1.76 (+0.03/-0.02) for the I channel, and β = 1.84 (+0.02/-0.03) for the I* channel. The TOF spectra for I*, and

corresponding integrated signal intensities of the dominant "forward" peak (t ~ 80 μs) for various polarization angles, are shown in Figs. 4 and 5, respectively. Additional polarization data including the determination of uncertainties in β are provided as supporting information. Assuming the photoionization efficiencies for propyl radicals, correlated to the two different I atom electronic states, are the same, the relative contributions to the m/e = 43 TOF data provides the I:I* branching ratio. As a second independent cross-check, TOF data for m/e = 127 (I and I*), m/e = 43 (C_3H_7), and m/e = 42 (C_3H_6), were recorded using 70 eV electron impact ionization. The I:I* branching ratios were thus independently derived in a second manner by assuming that the 70 eV ionization cross sections for I and I* detected at m/e = 127 were the same. The validity of this assumption is discussed further below. The analysis of the m/e = 43 TOF (C_3H_7) for both channels using electron impact ionization provided a third independent determination of the I:I* branching ratio. Good agreement was observed between the branching ratios derived from the three independent methods. For 1-C_3H_7I, we observed negligible C_3H_7 spontaneous secondary unimolecular decomposition, consistent with previous results.[8] The I* yield was found to be 76 ± 2 % for 1-iodopropane at 266 nm, with no evidence for β dependence on the product translational energy. We found no HI + C_3H_6 products from 1-C_3H_7I (yield < 0.21%).

A small contribution could be observed from photodissociation of van der Waals clusters. This signal, which was minimized by photolyzing the earlier warm part of the molecular beam pulse, could be observed in polarization experiments where the signals from monomer photodissociation were very small, e.g., when the photodissociation laser polarization was close to perpendicular to the detector axis. Separate P(E)s, for 1-C_3H_7I and 2-C_3H_7I, were used to fit the cluster contribution to the experimental polarization angle TOFs, illustrated in Fig. 6. Both P(E)s were determined by assuming that the respective parent dimers undergo photodissociation at 266 nm to form the corresponding parent monomers, i.e, $(1\text{-}C_3H_7I)_2 \rightarrow 1\text{-}C_3H_7I + 1\text{-}C_3H_7I$, and $(2\text{-}C_3H_7I)_2 \rightarrow 2\text{-}C_3H_7I + 2\text{-}C_3H_7I$, respectively. The product monomers could be observed directly at their parent masses using electron impact or photoionization detection. We believe that the dominant "dimer contribution" under our experimental conditions is from daughter ions at m/e = 127 (for both 1-C_3H_7I and 2-C_3H_7I) and m/e = 128 (for 2-C_3H_7I). From the polarization angular distributions for cluster photodissociation, β ~ 0.75 for 1-C_3H_7I , and β ~ 0.35 for 2-C_3H_7I, respectively. It is important to note that the small signals attributed to clusters have no material impact on our analysis of the primary photochemistry of monomers.

Time-of-flight spectra for C_3H_7, I and I* from 2-C_3H_7I are shown in Fig. 7. The overall P(E) for the I + C_3H_7 channel (see Fig. 8) was derived from the I TOF spectra. Analysis of the TOF spectra for the C_3H_7 counterfragment indicated that most C_3H_7 recoiling from I survives its transit to the detector. However, the slowest C_3H_7, corresponding to the most vibrationally excited C_3H_7, was absent from the TOF due to spontaneous unimolecular decomposition. The contributions are denoted by the pink and black dotted lines in Fig. 8, denoted as I + C_3H_7 and I + stable C_3H_7. In Figs. 9 and 10, the TOF spectra and integrated signal intensity distributions for the I channel, respectively, are shown for various polarization angles. The anisotropy parameters were found to be 1.90 (+0.03/-0.04) for the dominant I + stable C_3H_7 channel and 1.94 (+0.02/-0.01) for the minor I* channel. We found that the anisotropy parameter for the slow I atoms correlated with C_3H_7 that underwent spontaneous unimolecular dissociation had a slightly reduced value, i.e., β = 1.85 (-0.04/+0.03). A third, very minor contribution exists for the I + C_3H_7 channel (~ 0.74% of the "total" I channel), and characterized by a highly perpendicular angular distribution, with β = -1.0 and producing a slightly larger maximum translational energy release.

For 2-C_3H_7I, since the I and I* product channels cannot be resolved from product TOF alone, determination of the I and I* P(E) distributions, β parameters, and the I:I* branching ratio requires a state-selective detection method, here photoionization. The relative detection sensitivity for I and I* using 9.6 eV photoionization detection (with the VUV laser tuned on and off the I resonance as noted above), was determined from the measured photoionization intensities for 1-C_3H_7I photodissociation. Using the I : I* branching ratios for 1-C_3H_7I (determined as described above using three independent methods), we derived the relative experimental detection sensitivity for I and I* under our exact experimental conditions. This relative I:I* detection sensitivity was then used along with the measured absolute signal levels for the separately-measured I and I* TOF distributions using photoionization to determine the I:I* branching ratio for 2-C_3H_7I. We used the same approach to determine the I:I* ratios for CH_3I and C_2H_5I photodissociation and obtained I:I* branching ratios in agreement with those reported by others in the literature.[11]

The TOF spectra for HI from 2-iodopropane, recorded using electron impact ionization at 70 eV, are shown in Fig. 11. The HI elimination product angular distributions were found to be strongly anisotropic, with β = 1.94 (+0.04/-0.06) (see Fig. 12 and Fig. 13). Using electron impact ionization, the relative signal levels at HI^+ (m/e = 128) and I^+ (m/e = 127) were used to determine the HI:(I+I*) branching ratio, assuming that the 70 eV ionization cross sections for I and I* are the same. As discussed by Krajnovich et al, a simple empirical relation between ionization cross sections and polarizability is commonly used in determing branching ratios.[30] In the present case, the calculated polarizibities of I and I* are nearly the same,[31] and the I and HI electron impact ionization cross sections are available.[32] We used 6.13 Å^2, 5.91 Å^2 and 5.91 Å^2 for HI, I* and I, respectively. Experimental studies of HI electron impact ionization at 75 eV, close to that used in our experiment, indicate a 45:55 ratio for I^+:HI^+.[33]

The I:I*:HI branching ratio was found to be 0.240:0.760:<0.0021 for 1-iodopropane and 0.741:0.154:0.105 for 2-iodopropane. Thus, for 1-iodopropane, the photodissociation dynamics are very similar to those for methyl iodide and ethyl iodide,[11,12] producing ~ 74% I* at 266 nm, with no evidence for HI

production. On the other hand, for 2-iodopropane, a large shift is observed towards dominant production of ground state I, as well as a significant yield of HI. Note that we used an HI:I fragmentation ratio for room temperature HI to determine the HI yield.[33] As discussed below, there is strong evidence for significant HI vibrational excitation, likely increasing fragmentation of HI to I^+ upon 70 eV electron impact ionization relative to a room temperature sample. Therefore, we believe that our measured HI yields actually represent *lower limits* to the true HI yields.

We have also carried out preliminary studies involving the photodissociation of t-butyl iodide at 266 nm.[34] From these experiments, we have determined the I:I*:HI branching ratio for t-butyl iodide to be approximately 0.693:0.076:0.231. Clearly, the further increase in branching for 3° iodoalkanes leads to an even greater degree of nonadiabatic behavior producing even less I*, together with a significant increase in HI yield (to ≥ 23.1%). We note that the increase in nonadiabatic behavior with increased hydrocarbon branching in iodoalkanes has been reported a number of times in the past.[3,13,14,15] As illustrated in Fig. 11, the dominant contribution at m/e = 42 ($C_3H_6^+$) is nascent C_3H_6 from the HI + C_3H_6 channel, with additional contributions from spontaneous secondary decomposition of C_3H_7, and fragmentation of C_3H_7 upon ionization.

The TOF spectra for HI from photodissociation of 2-iodopropane, recorded using 9.9 eV photoionization - as well as using 9.6 eV photoionization - could be fit using the *same* P(E) derived from electron impact ionization data. Since, the 0 K ionization energy of HI is 10.38 eV, single photon ionization of HI at 9.9 eV is only possible for HI at v ≥ 2. From the HI + C_3H_6 translational energy distribution shown in Fig. 8, the most probable translational energy (20 kcal/mol) leaves ~67 kcal/mol of internal excitation in the HI + C_3H_6 products. Therefore, *very significant* HI vibrational excitation seems highly likely. Our ability to ionize HI at 9.6 and 8.8 eV (the latter yielding a P(E) similar but with a slightly smaller maximum translational energy release) might be taken as evidence for significant yields of HI (v > 3) and HI (v > 5), respectively. However, the known VUV absorption spectrum of HI reveals the existence of sharp, very strong absorption features at 9.6 and 8.8 eV, assigned to bound Rydberg states of HI,[35] possibly facilitating resonance-enhanced 2-photon ionization. Thus, while our results strongly suggest a large yield of HI (v ≥ 2), more definitive conclusions regarding the populations of higher HI vibrational levels await further experimental studies.

Our finding that HI elimination plays an important role in 2-iodopropane and t-butyl iodide — but not for 1-iodopropane — is consistent with the qualitative conclusions by Ross and Johnston.[17] In their study, the relative branching fractions for the HI product channel in primary, secondary and tertiary Iodoalkanes were not determined. However, it was suggested that the expected branching fractions, for the 1,2-HI elimination process, might reflect the statistical abundance of the available secondary H atoms (bonded to the C_β atoms) in those Iodoalkanes. The ratio is 2:6:9 for 1-C_3H_7I, 2-C_3H_7I, and t-C_4H_9I, respectively. However, since we find that the HI yield from 1-iodopropane is ~ 50 times smaller than that from 2-iodopropane (rather than a factor of 3), the strong isomer dependence of the HI yield *cannot* simply reflect statistical secondary H atom abundances.

For photodissociation of 2-iodopropane, the HI P(E) and β parameter closely resemble corresponding values for ground state I ($^2P_{3/2}$). Similar behavior was seen in the photodissociation of t-butyl iodide.[34] Assuming a pure parallel transition, in the axial recoil limit, a reduction of β from the limiting value of 2.0 will occur when the excited state lifetime (τ) is sufficiently long to allow some parent rotation prior to product formation. For a parallel transition with photofragment recoil along the transition dipole axis, the dependence of β on parent lifetime (τ), using a pseudodiatomic model for polyatomic molecules, is given by[29]

$$\beta = \frac{1}{2}(1 + 3\gamma e^{\gamma} \int_{\gamma}^{\infty} \frac{e^{-v}}{v} dv) \qquad (2),$$

where

$$\gamma = \frac{I}{8kT\tau^2} \qquad (3)$$

Here, I is the relevant moment of inertia in the parent molecule relevant for product formation, k is the Boltzmann constant, T is the rotational temperature of the parent molecules, and τ is the average lifetime of the parent molecules prior to dissociation. As a first order approximation, Eqns. 2 and 3 can be used together to predict how β will decrease from 2.0 with increasing τ, in the dissociation of 2-iodopropane. Conversely, for a given measured value of β, one can calculate a corresponding average dissociation lifetime (τ) for a particular rotational temperature. This is plotted in Fig. 14 for β = 1.94, the value measured for HI elimination in our experiment. We used I = 3.38 x 10^{-45} kg m^2 for HI elimination, which is taken to be the same as for C-I bond fission. Assuming T = 10 K - which we estimate to be the temperature of the parent molecular beam - the expected timescale for the HI product formation is 0.36 ps. Even if we assume that T = 2 K, the expected HI dissociation timescale is ~ 0.81 ps. Since we used the earlier warm part of the alkyl iodide pulse to minimize cluster contributions, a rotational temperature below 2 K is highly unlikely. Thus, on the basis of our experimental observations, we conclude that HI elimination occurs on subpicosecond timescales, similar to direct C-I bond fission.

In the above calculations, we have used β = 1.94. However, a small contribution at 266 nm from direct absorption to either the $^3Q_1$ or $^1Q_1$ states, involving perpendicular transitions (β = -1.0), would also cause the small reduction of β from 2.0 observed in this study. Thus, dissociation timescales considerably smaller than 0.36 ps are certainly possible. From these considerations, our measured values of β are entirely consistent with dissociation timescales measured by Corrales and coworkers, who used femtosecond pump-probe

techniques to directly measure τ = 0.137 ps for C-I bond fission in 2-iodopropane photodissociation at 268 nm.[12]

As in C-I bond fission, HI elimination appears to occur directly on repulsive excited potentials on sub-picosecond timescales. This suggests that the motion of the heavy I atom in HI is largely derived from the repulsive nature of the $^1Q_1$ potential energy surface correlating to R + I, with the heavy I atom picking up a light H atom late in the exit channel. Because the I ($^2P_{3/2}$) yield is significant (24%) for 1-iodopropane, the absence of HI production for this isomer indicates that nonadiabatic crossing to $^1Q_1$ is not sufficient for HI production.

Carbon-halogen (C-X) bond fission in the photodissociation of *unsaturated* halogen-substituted hydrocarbons usually occurs directly on excited state potential energy surfaces, whereas HX elimination usually proceeds on the ground electronic state surfaces following internal conversion.[18-22] The large values of β for HI elimination observed in our study clearly indicate that the timescales for HI elimination are subpicosecond, comparable to those for primary C-I bond fission, which has been measured to be ~ 0.137 ps.[12] For polyatomic molecules in this size range, dissociation on the ground electronic state PES through internal conversion leads to significantly longer dissociation timescales,[36] which would be expected to produce a large reduction in β from 2.0.[29] For example, the angular distributions of HX from UV-excited vinyl halides are usually nearly isotropic, i.e., $\beta \sim 0$.[19] However, in rare cases, HX elimination on excited state surfaces of unsaturated alkyl halides has been observed. In femtosecond pump-probe studies of allyl chloride photodissociation, two-timescales were observed for HCl elimination (600 fs and 14 ps). These were attributed to mechanisms involving direct dissociation and internal conversion, respectively.[21] To our knowledge the only observation of HX elimination in *saturated* halocarbons occurring on excited state potential energy surfaces involved HCl elimination from CH_3Cl following excitation at 157 nm.[23] In that case, two channels were observed, involving formation of ground state triplet methylene ($^3CH_2$) as well as electronically excited singlet methylene ($^1CH_2$). The translational energy distributions for $^3CH_2$ + HCl suggested a direct excited state mechanism, whereas $^1CH_2$ +HCl appeared to involve internal conversion. Clearly, the similarity of the HI and I($^2P_{3/2}$) P(E)s and β values for both 2-iodopropane and t-butyl iodide suggests that the HI elimination dynamics are intimately tied to direct C-I bond fission on an excited state potential energy surface, rather than via internal conversion.

We now consider the possible mechanistic details for HI elimination from branched iodoalkanes. For iodoalkane *thermal decomposition,* involving HI elimination on *ground electronic state potential energy surfaces*, the relative HI yields follow the order 1° RI < 2 ° RI < 3 ° RI. This is expected since the potential energy barrier heights for formation of HI product molecules are greatest for primary Iodoalkanes, intermediate for secondary Iodoalkanes, and least for tertiary Iodoalkanes.[37,38,39,40] From studies of the thermal decomposition of alkyl halides, it has been concluded that transition states for HX elimination from alkyl halides (or HX addition to alkenes) have appreciable (~ 50%) ion-pair R^+X^- character.[36-38] Thus, trends in barrier heights for HX elimination have been attributed to the stabilities of carbocation intermediates, which increase in the order 1° R^+ < 2° R^+ < 3° R^+ due to the greater polarizability of alkyl groups compared to hydrogen, and to the increasing role of hyperconjugation with branching. By analogy, similar arguments might potentially explain the observed isomer dependence of the HI yields in the photodissociation of alkyl iodides. However, since HI elimination appears to be a direct process with β and P(E) distributions remarkably similar to those for the I channel, it is important to explore dynamical origins for the observed strong isomer dependence of HI yield.

The primary nuclear motion imparted to the hydrocarbon fragment during C-I bond fission is expected to play an important role in the subpicosecond elimination of HI. Corrales and coworkers studied the photodissociation of a series of alkyl iodides using femtosecond time resolved velocity map imaging of the I and I* products.[12] Full-dimension time-resolved dynamics calculations, presented as movies posted as supplemental information on the PCCP website, supported their experimental measurements. As illustrated in the screenshots of the movies, shown in Fig. 15, a significant difference exists between the photodissociation of 1-C_3H_7I and the branched alkyl iodides such as 2-C_3H_7I and t-butyl iodide. For 1-C_3H_7I, C-I bond fission involves a large exit impact parameter relative to the center of mass of the hydrocarbon fragment, leading to significant rotational excitation. This produces arc-like motion of the secondary H atoms, nearly orthogonal to the reaction coordinate for HI bond formation. For photodissociation of branched compounds, on the other hand, the near-zero impact parameter half collision produces very significant bending excitation at the α-carbon atom. This umbrella-like bending motion directs the secondary H-atoms towards the departing I atom, close to the axis of the half-vacant p-orbital, thereby favouring HI formation. Since this process is likely to be operational over relatively long H-I distances, significant HI vibrational excitation appears to be highly likely, consistent with our ability to ionize HI well below the 0 K threshold of 10.38 eV. We note that ground state I + H correlates to the stable ground electronic state of HI, whereas excited I* + H correlates only to repulsive and weakly bound excited states of HI.[41] This is highly consistent with the observation that HI P(E) distributions closely resemble those for I rather than for I*.

The relatively significant yields of HI from the 266 nm photolysis of the branched iodoalkanes 2-iodopropane and t-butyl iodide, are quite remarkable in light of the absence of this channel for 1-iodopropane. In this article, we suggest that this interesting isomer-selectivity can likely be traced to differing initial nuclear motions imparted by primary C-I bond fission. New dynamical calculations would be extremely valuable to better understand the photoinduced ultrafast HI elimination from alkyl iodides.

Conclusions

HI elimination was found to play a significant role in the photodissociation dynamics of branched iodoalkanes at 266 nm. Strongly anisotropic product angular distributions indicate that HI elimination occurs on subpicosecond timescales, and consequently, that it occurs directly on excited state potential energy surfaces. The similarity between the HI and ground state I translational energy distributions suggest that a close connection exists between these channels, with the departing I atom picking up a light H atom late in the exit channel, leading to significant HI vibrational excitation. These direct excited state dynamics contrast the usual behavior for HX elimination from halogenated hydrocarbons, which typically proceed on ground electronic state surfaces following internal conversion.

Conflicts of interest

There are no conflicts to declare.

Acknowledgements

This research was supported by the Office of Science, Basic Energy Sciences, U.S. Department of Energy, under Grant No. DE-FG02-00ER15095. The development of some of the laser methods for VUV generation and REMPI schemes for I atom detection, were supported in part by a grant from the National Science Foundation, CHE-1301156.

References

1 A.B. Alekseyev, H.P. Liebermann, R.J. Buenker, S.N. Yurchenko, *J. Chem. Phys.*, 2007, **126**, 234102.
2 S.J. Riley, K.R. Wilson, *Faraday Disc. Chem. Soc.*, 1972, **53**, 132-146.
3 F.G. Godwin, C. Paterson, P.A., Gorry, *Mol. Phys.*, 1987, **61**, 827-848.
4 C. Paterson, P.A., F.G. Godwin, Gorry, *Mol. Phys.*, 1987, **60**, 729-747.
5 R.K. Sparks, K. Shobatake, L.R. Carlson, Y.T. Lee, *J. Chem. Phys.*, 1981, **75**, 3838-3846.
6 R.E. Continetti, B.A. Balko, Y.T. Lee, *J. Chem. Phys.*, 1988, **89**, 3383-3384.
7 A.T.J.B. Eppink, D.H. Parker, *J. Chem. Phys.,* 1998, **109**, 4758-4767.
8 H. Fan, S.T. Pratt, *J. Chem. Phys.*, 2005, **123**, 204301.
9 V.A. Shubert, M. Rednic, S. T. Pratt, *J. Chem. Phys.*, 2009, **130**, 134306.
10 H. Fan, S.T. Pratt, *J. Chem. Phys.*, 2006, **124**, 114312.
11 S.H. Gardiner, M.L. Lipciuc, T.N.V. Karsili, M.N.R. Ashfold, C. Vallance, *Phys. Chem. Chem. Phys.*, 2015, **17**, 4096-4106.
12 M.E. Corrales, V. Loriot, G. Balerdi, J. Conzalez-Vazquez, R. de Nalda, L. Banares, A.H. Zewail, *Phys. Chem. Chem. Phys.*, 2014, **16**, 8812-8818.
13 Y.S. Kim, W.K. Kang, D.C. Kim, K.H. Jung, *J. Phys. Chem. A.*, 1997, **101**, 7576-7581.
14 Y. Liu, Q. Zheng, Y. Zhang, R. Zhang, Y. Wang, B. Zhang, *Chem. Phys. Chem.*, 2009, **10**, 830-834.
15 F. Zhang, Y.M. Wang, B. Zhang, W.L. Feng, *Acta. Phys. Chim. Sin.*, 2010, **26**, 1903-1908.
16 C.M. Roehl, J.B. Burkholder, G.K. Moortgat, A.R. Ravishankara, P.J. Crutzen, *J. Geophys. Res.*, 1997, **102**, 12819-12829.
17 P.L. Ross, M.V. Johnston, *J. Phys. Chem.*, 1995, **99**, 4078-4085.
18 P. Zou, K.E. Strecker, J. Ramirez-Serrano, L.E. Jusinski, C.A. Taatjes, D.L. Osborn, *Phys. Chem. Chem. Phys.*, 2008, **10**, 713-728.
19 S. Pandit, B. Hornung, and A.J. Orr-Ewing, *Phys. Chem. Chem. Phys.*, 2016, **18**, 28353.
20 M. Kawasaki, K. Kasatani, H. Sato, *Chem. Phys.*, 1984, **88**, 135-142
21 H. Shen, J. Chen, L. Hua, B. Zhang, *J. Phys. Chem. A*, 2014, **118**, 4444-4450.
22 S.H. Lee, W.K. Chen, C. Chaudhuri, W.J. Huang, *J. Chem. Phys.*, 2006, **125**, 144315.
23 J.J. Lin, Y. Chen, Y.Y. Lee, Y.T. Lee, X. Yang, *Chem. Phys. Lett.*, 2002, **361**, 374-382.
24 X. Yang, J. Lin, Y.T. Lee, D.A. Blank, A.G. Suits, A.M. Wodtke, *Rev. Sci. Instrum*., 1997, **68**, 3317-3325.
25 D.R. Albert, D.L. Proctor, H.F. Davis, *Rev. Sci. Instrum.*, 2013, **84**, 063104.
26 D.R. Albert, H.F. Davis, *Phys. Chem. Chem. Phys.*, 2013, **15**, 14566-14580.
27 D.L. Proctor, D.R. Albert, H.F. Davis, *Rev. Sci. Instrum.* **81**, 023106 (2010).
28 SBEAM is Cornell variant of the program CMLAB2 used for analysis of photodissociation data; Zhao, X, Ph.D. Dissertation, University of California, Berkeley, 1988. We have verified that both programs yield the same results.
29 S. Yang and R. Bersohn, *J. Chem. Phys.*, 1974, **61**, 4400-4406.
30 D. Krajnovich, L.J. Butler, Y.T. Lee, *J. Chem. Phys.*, 1984, **81**, 3031-3047.
31 T. Fleig and A.J. Sadlej, Phys. Rev. A, 65, 032506 (2002).
32 M. Vindodkumar, R. Dave, H. Bhutadia, and B.K. Antony, Int. J. Mass Spec. 292, 7 (2010).
33 H. K. Nasrallah, P. Marmet, and R. Dutil, *Int. J. Mass Spec. Ion Proc.* **55**, 1 - 14 (1983/1984).
34 S. Datta, M. Todt, H. F. Davis, to be published.
35 C.E. Brion, M. Dyck, G. Cooper, *J. Electr. Spectr. Rel. Phenom.*, 2005, **144-147**, 127-130.
36 R.D. Levine, *Molecular Reaction Dynamics*, Cambridge

University Press, 2009.
37 K.H. Weber, J.M. Lemieux, J. Zhang, *J. Phys. Chem. A*, 2009, **113**, 583-591.
38 A. Miyoshi, N. Yamauchi, K. Kosaka, M. Koshi, H. Matsui, *J. Phys. Chem. A*, 1999, **103**, 46-53.
39 S.W. Benson, A.N. Bose, *J. Chem. Phys.*, 1963, **39**, 3463-3473.
40 A. Maccoll, *Chem. Rev.*, 1969, **69**, 33-60.
41 A.B. Alekseyev, H.-P: Liebermann, D.B. Kokh and R.J. Buenker, *J. Chem. Phys.* **113**, 6174 (2000).

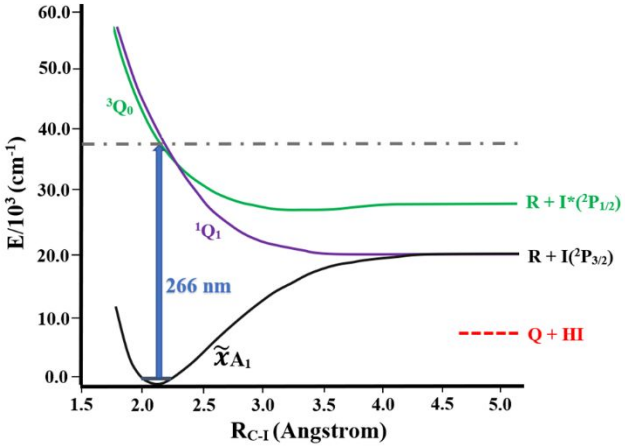

Fig. 1: *Potential energy diagram for 266 nm photodissociation of iodoalkanes.*

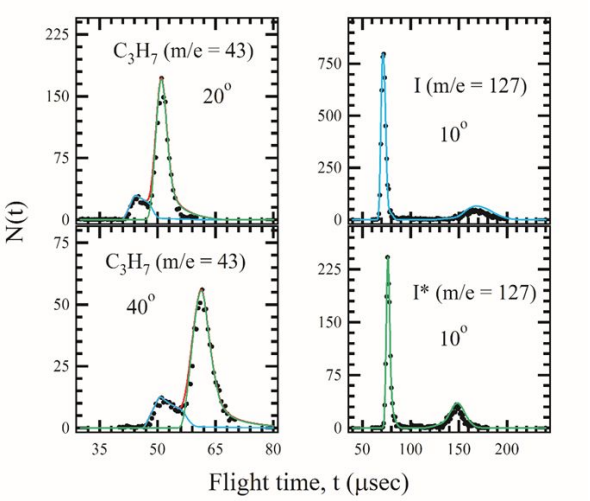

Fig. 2: *Time-of-flight spectra for C_3H_7, I, and I* from photodissociation of 1-C_3H_7I at indicated lab angles: the black dots are the experimental data; the blue lines are calculated TOFs for the I + C_3H_7 channel; the green lines are calculated TOFs for the I* + C_3H_7 channel. The corresponding P(E)s are depicted in Fig. 3.*

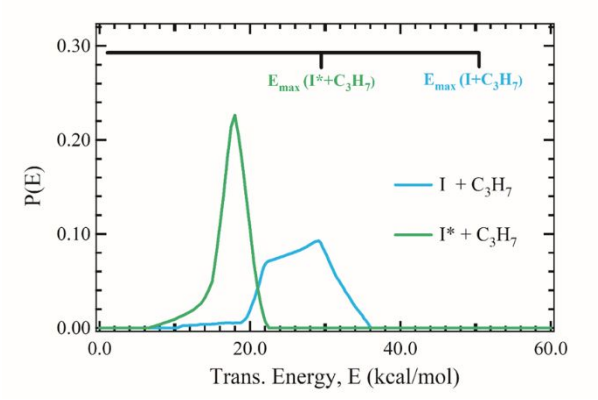

Fig. 3: *Translational energy distributions for I + C_3H_7, and I* + C_3H_7 from photodissociation of 1-C_3H_7I.*

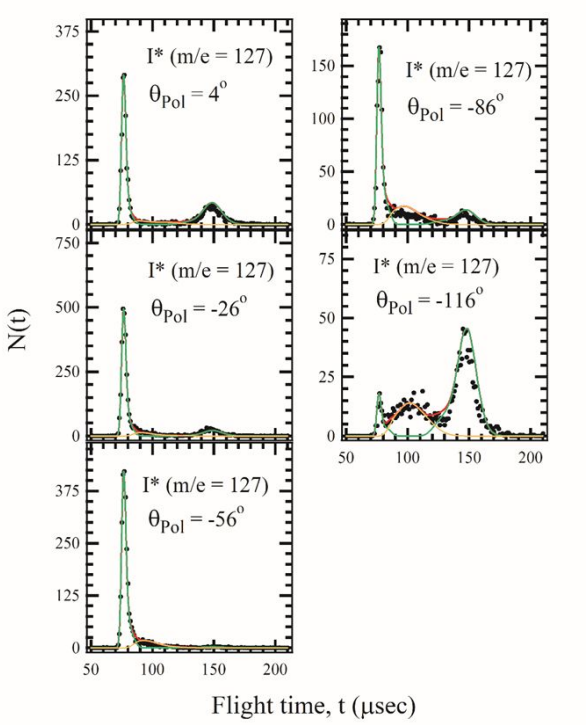

Fig. 4: *Time-of-flight spectra for I* from 1-C_3H_7I photodissociation, at their indicated polarization angles. The green lines are calculated for the I* + C_3H_7 channel; the orange lines are calculated for the 1-C_3H_7I cluster photodissociation channel. The red lines correspond to the calculated overall TOFs. The P(E)s are depicted in Figs. 3 and 6.*

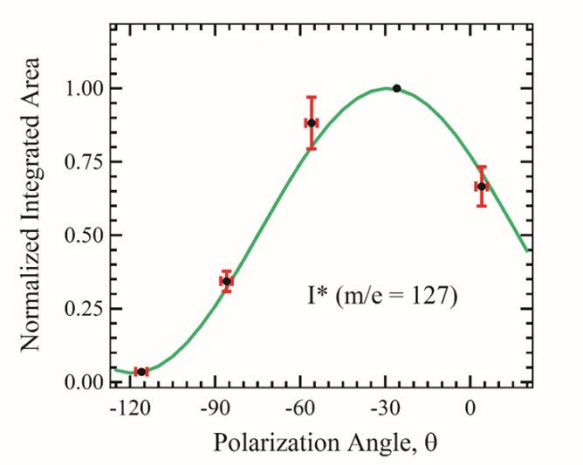

Fig. 5: *Normalized integrated polarization angular distribution at lab angle of 10°, for I* + C_3H_7 from 1-C_3H_7I photodissociation: the black dots correspond to the integrated TOF from Fig. 4; the error bars are shown in red; the green line corresponds to the calculated distribution for* β = 1.84 (+0.02/-0.03).

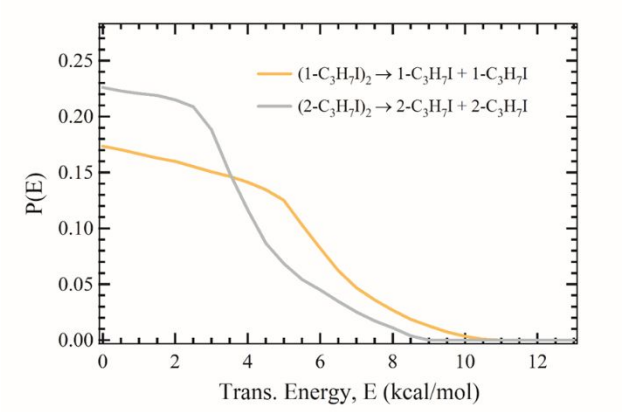

Fig. 6: *Translational energy distributions for cluster photodissociation for 1-C_3H_7I, and 2-C_3H_7I,.*

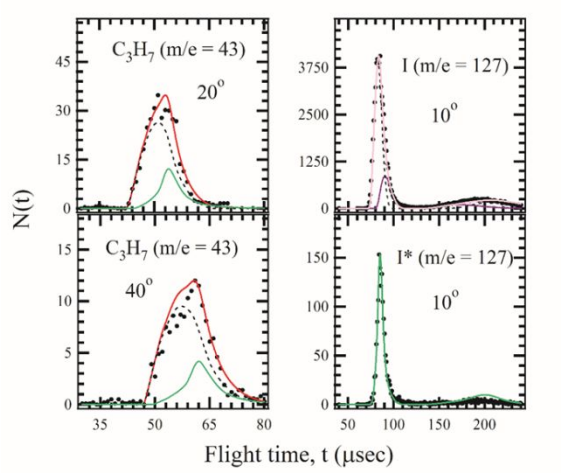

Fig. 7: *Time-of-flight spectra for C_3H_7, I, and I* from 2-C_3H_7I, at indicated lab angles using photoionization detection. The red lines correspond to the calculated overall C_3H_7 TOFs while the pink line corresponds to the calculated overall TOF for I. The black dashed lines are calculated TOFs for I + stable C_3H_7; the purple lines correspond to calculated TOFs for I + unstable C_3H_7; the green lines are TOFs for I* + C_3H_7, respectively. The corresponding P(E)s are depicted in Fig. 8.*

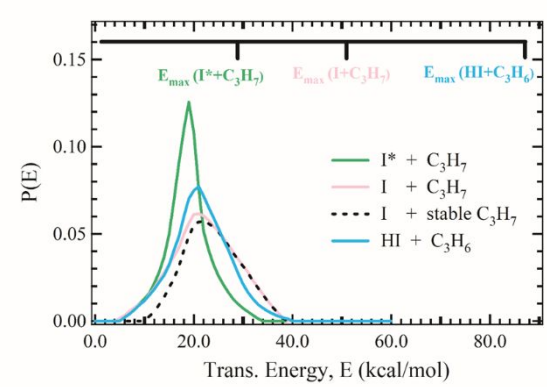

Fig. 8: *Translational energy distributions for products from photodissociation of 2-C_3H_7I.*

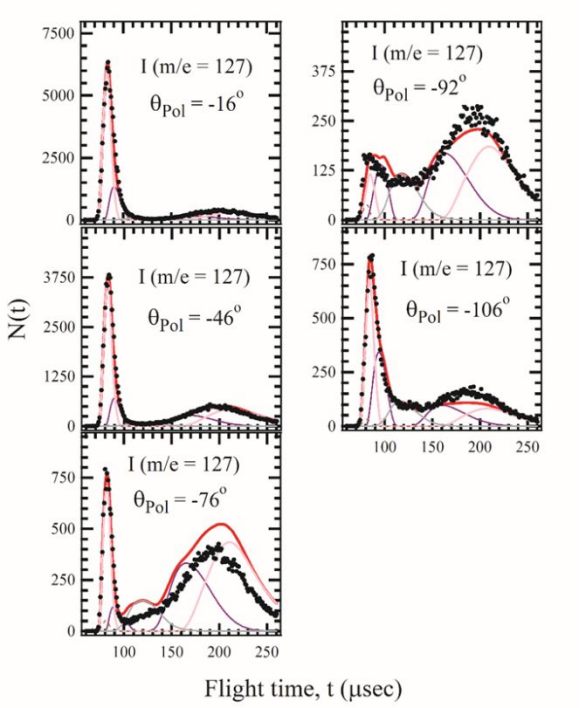

Fig. 9: *Time-of-flight spectra (10°) for I from 2-C_3H_7I photodissociation, at indicated polarization angles: the pink lines correspond to the calculated TOFs for I + stable C_3H_7; the purple lines correspond to calculated TOFs for I + unstable C_3H_7; the brown dashed lines correspond to the calculated TOFs for I + perpendicular C_3H_7; the gray lines are calculated TOFs for 2-C_3H_7I cluster photodissociation, respectively. The P(E)s are depicted in Figs. 8 and 6.*

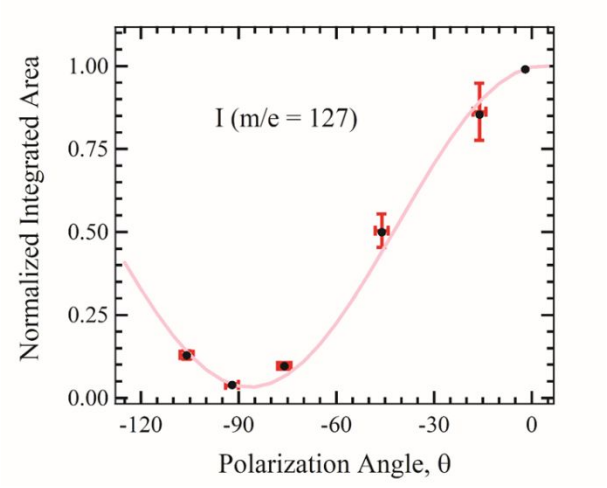

Fig. 10: *Integrated polarization angular distribution, at a lab angle of 10°, for the I + stable C_3H_7 channel from 2-C_3H_7I photodissociation (Fig. 9)- the pink line corresponds to the calculated distribution for β = 1.90 (+0.03/-0.04).*

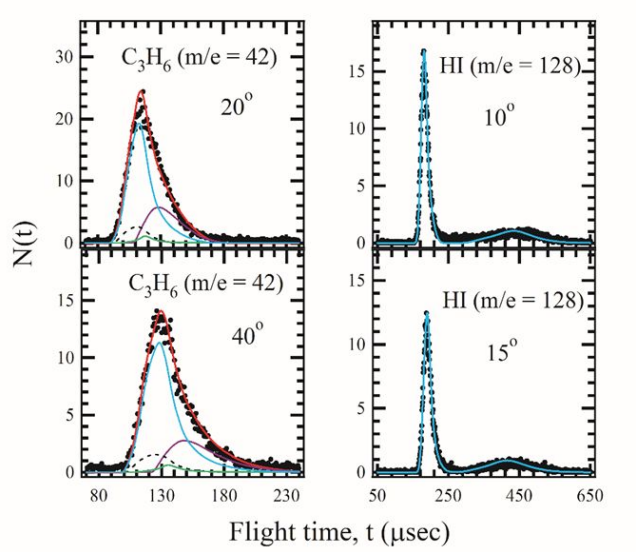

Fig. 11: *Time-of-flight spectra for C_3H_6 and HI from photodissociation of 2-C_3H_7I at indicated lab angles. The blue lines are calculated TOFs for HI + C_3H_6; the black dashed lines correspond to the calculated TOFs for C_3H_6 daughter ions from I + stable C_3H_7; the purple lines are C_3H_6 from I + unstable C_3H_7; the green lines correspond to fragmentation from the I* + C_3H_7 channel, respectively. The P(E)s are depicted in Fig. 8.*

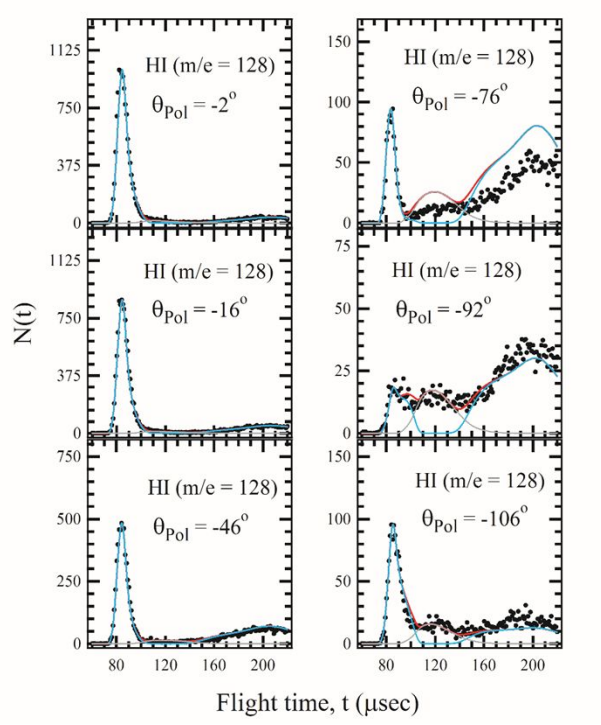

Fig. 12: *Time-of-flight spectra for HI from 2-C_3H_7I at indicated polarization angles. The blue lines correspond to the HI + C_3H_6 channel; the gray lines are for the 2-C_3H_7I cluster photodissociation. The P(E)s are depicted in Figs. 8 and 6.*

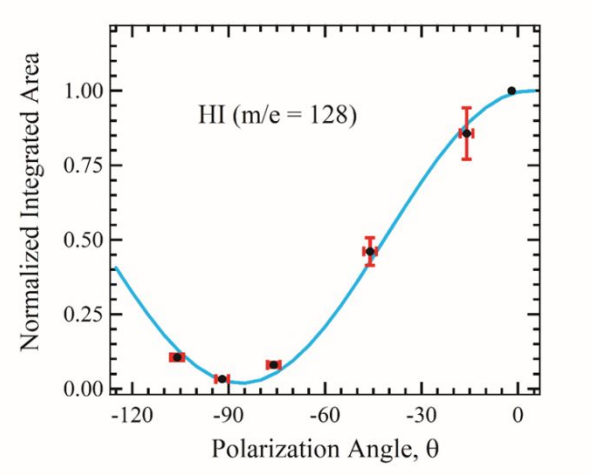

Fig. 13: *Integrated polarization angular distribution, at a lab angle of 10°, for the HI + C_3H_6 data (Fig 12) for 2-C_3H_7I photodissociation: the blue line corresponds to the calculated distribution for β = 1.94 (+0.04/-0.06).*

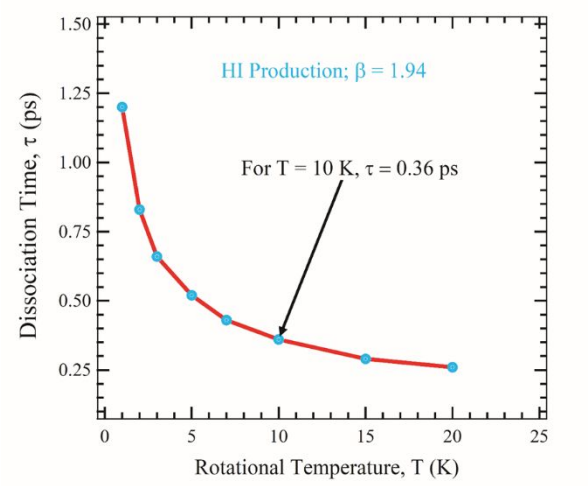

Fig. 14: *Plot of parent unimolecular dissociation time vs. rotational temperature for 2-C_3H_7I, assuming β = 1.94. For T = 10 K, the calculated dissociation time is 0.36 ps.*

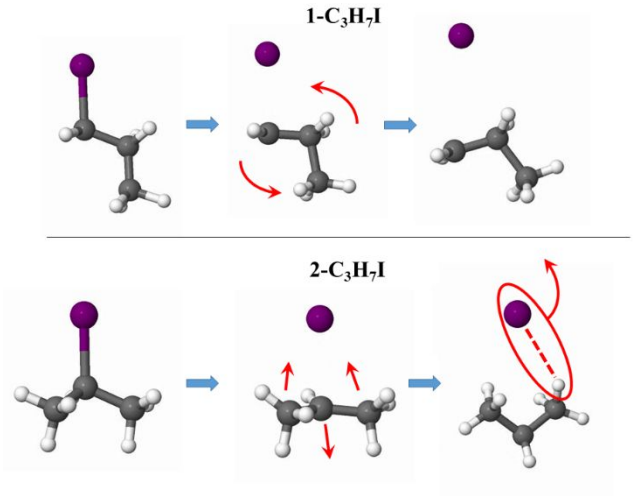

Fig. 15: *Screenshots from movies of on-the-fly trajectories for direct C-I bond fission in 1-C_3H_7I and 2-C_3H_7I photodissociation, accompanying the paper by Corrales et. al. (ref. 12). For 1-C_3H_7I, C-I bond fission leads to hydrocarbon rotational excitation with secondary H atom motion nearly orthogonal to the reaction coordinate for HI bond formation. For 2-C_3H_7I, umbrella-like bending excitation at the central carbon atom causes the secondary H atoms to be presented to the departing I atom with motion closer to the reaction coordinate for HI bond formation.*

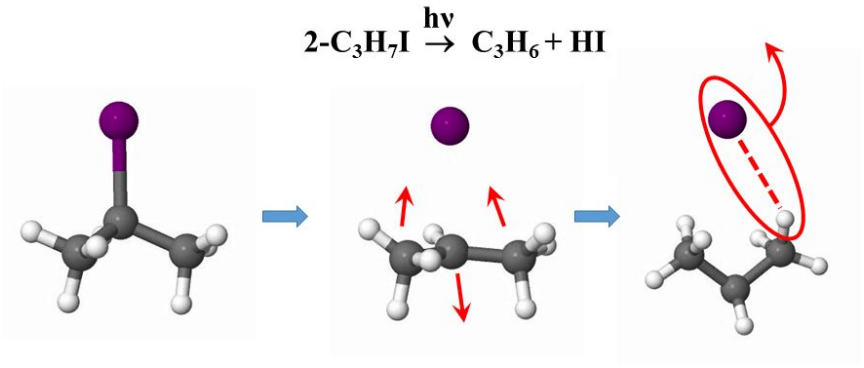

TOC Caption: New experiments reveal a close connection between the nonadiabatic dynamics of C-I bond fission and HI elimination in the photodissociation of branched iodoalkanes.